GEOPHYSICS, VOL. 70, NO. 4 (JULY-AUGUST 2005); P. O13–O27, 14 FIGS.
10.1190/1.1993711

On the use of quasi-static deformation to understand reservoir fluid flow

Don W. Vasco[1] and Alessandro Ferretti[2]

ABSTRACT

Deformation above a producing reservoir provides a valuable source of information concerning fluid flow and flow properties. Quasi-static deformation occurs when the displacements are so slow that we may neglect inertial terms in the equations of motion. We present a method for inferring reservoir volume change and flow properties, such as permeability, from observations of quasi-static deformation. Such displacements may represent surface deformation such as tilt, leveling, interferometric synthetic aperture radar (InSAR), or bathymetry observations or subsurface deformation, as inferred from time-lapse seismic surveys. In our approach, the equation for fluid flow in a deforming reservoir provides a mapping from estimated fractional volume changes to reservoir permeability variations. If the reservoir behaves poroelastically over the interval of interest, all the steps in this approach are linear. Thus, the inference of reservoir permeability from deformation data becomes a linear inverse problem. In an application to the Wilmington oil field in California, we find that observed surface displacements, obtained by leveling and InSAR, are indeed compatible with measured reservoir volume fluxes. We find that the permeability variations in certain layers coincide with fault-block boundaries suggesting that, in some cases, faults are controlling fluid flow at depth.

INTRODUCTION

Production-related deformation of the material overlying a reservoir is typically ignored unless it becomes a serious problem. For example, for reservoirs near large bodies of water, subsidence can result in flooding and damage to surface facilities. Notable examples include the Wilmington oil field in California (Allen and Mayuga, 1969; Colazas and Strehle, 1994), the Oronoco Basin in Venezulea (Chilingarian et al., 1994), the Po Delta field in Italy, and the Groningen field in the Netherlands (Barends et al., 1995). Deformation in the overburden can be problematic for offshore fields, such as Ekofisk (Sulak, 1991), resulting in platform and equipment damage. It is well known that production-related deformation can induce seismic activity and lead to well failures (Rouffignac et al., 1995; Dale et al., 1996). Displacement of the overburden can also impact the interpretation of time-lapse reservoir monitoring. Time-lapse seismic monitoring is rapidly becoming a quantitative tool for imaging fluid saturation and pressure changes within a producing reservoir (Landro, 2001). Compactable reservoirs are ideal candidates for the application of time-lapse methods (Lumley et al., 1997), having high porosity and low dry-bulk modulus. However, the deformation in the overburden can be a significant contributor to time-lapse changes (Guilbot and Smith, 2002; Minkoff et al., 2004), masking saturation and pressure changes. Finally, deformation is intensively studied when porosity changes within a compacting reservoir result in a substantial loss of permeability, prematurely ending production.

Deformation due to production is typically quasi-static. That is, the movement is so slow that inertial terms in the equation of motion are negligible. Despite their rather direct relationship to pressure changes (Dussealt et al., 1993; Bruno and Bilak, 1994; Vasco et al., 1998; Du and Olson, 2001), quasi-static deformation data are rarely used to better understand flow within a reservoir. One exception to this is the use of tilt meters to characterize hydrofracture propagation (Evans et al., 1982; Palmer, 1990; Castillo et al., 1997). There may be several reasons for the limited use of deformation observations. First, in the past, techniques to measure deformation were relatively expensive. For example, leveling surveys over Wilmington field are a significant expense (Strehle 1996) and are probably only conducted because of the proximity of the field to the city of Long Beach. Similarly, tilt meters must be placed in shallow boreholes in order to reduce the effects of thermal variations, adding to the cost of deployment. Second, until recently, there were few

Manuscript received by the Editor February 18, 2004; revised manuscript received October 26, 2004; published online July 7, 2005.
[1]Lawrence Berkeley Laboratory, Earth Sciences Division, 1 Cyclotron Road, 90-1116, Berkeley, California 94720. E-mail: dwvasco@lbl.gov.
[2]Politecnico di Milano, Dipartimento di Elettronica e Informazione, Piazza Leonardo da Vinci, 32-20133 Milan, Italy. E-mail: alessandro.ferretti@treuropa.com.

cost-effective methods for accurately monitoring deformation associated with offshore fields. The primary method for offshore monitoring was bathymetry surveys (Chin and Nagel 2004), which are not typically conducted in a systematic fashion. Offshore fields constitute a large fraction of current petroleum production. Third, the analysis of internal deformation in a reservoir can be quite complicated. Thus, extensive modeling may be necessary in order to capture the processes at play in the reservoir. Finally, there is a general sense that deformation within a reservoir is rather small, a notion that is reinforced by the paucity of observations.

Recent developments suggest that deformation above a producing reservoir can be measured efficiently and with high resolution. In particular, interferometric synthetic aperture radar (InSAR) is a satellite-based method which can provide accurate (subcentimeter) estimates of surface deformation at high resolution (20 m $\times$ 20 m pixels) (Bamler and Hartl, 1998). Images are available for much of the Earth's surface on a roughly month-by-month basis. With additional satellites, the return time could be reduced to weeks or days. The introduction of recent approaches based on long temporal series of radar data, such as the permanent scatterers (PS) technique, has significantly improved estimates of range change (Ferretti et al. 2000). Downhole tilt meters are now available (Wright, 1998; Wright et al., 1998) and may be used in slim holes to monitor reservoir deformation at depth. Time-lapse seismic observations are sensitive to production-induced deformation and can be used to infer displacement of the overburden even in offshore fields (Guilbot and Smith, 2002). Finally, it may be possible to use acoustic positioning or interferometric multibeam sonar measurements of the displacement of the sea floor, allowing for studies in offshore regions (Spiess et al., 1998; Chang et al., 2000).

In this paper, we demonstrate the utility of quasi-static displacement data for understanding flow within a reservoir. In particular, we use quasi-static deformation data to infer permeability variations within a reservoir. The methodology is based upon work presented in Vasco et al. (2001). Recently, this technique has been used to image permeability variations using time-lapse seismic-pressure estimates (Vasco, 2004). Our approach is applicable to any measure of deformation, such as displacement, tilt, strain, satellite-range change, and time-lapse seismic estimates. We apply the method to a set of permanent scatterer measurements gathered over the Wilmington oil field (Colesanti et al., 2003). These measurements are very accurate (on the order of a few millimeters), high-resolution estimates of surface displacement derived from InSAR data (Ferretti et al., 2000, 2001). We examine the compatibility of measured reservoir volume fluxes (caused by production and injection) with observed surface deformation.

METHODOLOGY

Governing equations

In this section, we outline the equations governing the physical processes in a deforming reservoir. Because of the coupled nature of fluid flow and reservoir deformation and the wide range of possible behaviors, such descriptions can rapidly become complicated. We present only what is necessary for understanding the processes at work. In particular, we consider only poroelastic and poroplastic rheologies for the reservoir proper. The overlying medium, outside the reservoir, will be considered to behave elastically. Also, we do not distinguish between fluid types within the reservoir. Thus, fluid pressure is described by a single equation for an average fluid. This is not a limitation of the method. Rather, in an application to data from the Wilmington oil field, we do not have detailed information concerning the fluid fluxes in the reservoir. Also, Wilmington field has been extensively waterflooded and has a long production history. Thus, the saturation distribution within the field is complicated, and the fluids are probably rather well mixed. The discussion proceeds in two stages: first, describing flow within a deforming reservoir and second, calculating deformation in an elastic overburden.

Fluid flow within a deforming reservoir

Fluid flow within the reservoir is governed by the equation of continuity for an incompressible fluid in a deformable reservoir (de Marsily, 1986, p. 85):

$$\nabla \cdot \mathbf{U} + \frac{\partial \phi}{\partial t} + q = 0, \tag{1}$$

where $\mathbf{U}$ denotes the filtration velocity of the fluid, ϕ is the porosity, and q is a source or sink term. Equation 1 is combined with Darcy's law, the constitutive equation relating the fluid velocity to the pore-fluid pressure gradient (de Marsily, 1986),

$$\mathbf{U} = -\frac{k}{\mu}(\nabla p + \rho g \mathbf{z}), \tag{2}$$

where k is the intrinsic permeability, μ is the dynamic viscosity of the fluid, p is the fluid pressure, ρ is the density, g is the gravitational acceleration, and $\mathbf{z}$ is a vector pointing in the direction of the local gravity field. Substituting equation 2 into equation 1 gives

$$\frac{\partial \phi}{\partial t} - \nabla \cdot \left[\frac{k}{\mu}(\nabla p + \rho g \mathbf{z})\right] + q = 0. \tag{3}$$

The rheological behavior of the reservoir is implicit in equation 3. Specifically, in order to relate the porosity to the pore fluid pressure p, one must specify the mechanical behavior of the reservoir. For example, for a poroelastic reservoir, the relationship is linear (Biot, 1941; Audet and Fowler, 1992):

$$\phi - \phi_0 = \frac{1}{Q} p + \frac{3\alpha(1-2\nu)}{2G(1+\nu)}(P - \alpha p), \tag{4}$$

which involves the initial porosity ϕ_0, the bulk (or overburden) pressure P, and four elastic constants: G (shear modulus), ν (Poisson's ratio), α (Biot's constant), and Q, which is another material constant.

For a poroplastic reservoir, the relationship between porosity and pore-fluid pressure is nonlinear (Audet and Fowler, 1992). Perhaps the most significant qualitative difference between poroelastic and poroplastic behavior is the irreversible nature of poroplastic deformation. That is, the volume changes associated with pressure increases will generally differ from those corresponding to pressure decreases. The relationship between pore volume and, hence, fluid volume and pressure is usually defined in terms of the effective pressure, p_e, which is the difference between the bulk and fluid

pressures:

$$p_e = P - p. \tag{5}$$

Generally, we will have an equation, such as

$$p_e = P - p = F(\phi), \tag{6}$$

where $F(\phi)$ is a relationship derived from laboratory measurements made on core samples (Chen and Mizuno, 1990; Audet and Fowler, 1992). Note that equation 6 is specific to a particular rock type and pore fluid. That is, for the entirely general situation, equation 6 depends on the lithology and the pore-fluid properties, among other things. In what follows, we assume that the lithology and pore-fluid properties are fixed. Rearranging equation 6 and substituting it into equation 3 results in

$$\frac{\partial \phi}{\partial t} + \nabla \cdot \left[\frac{k}{\mu} \left(\frac{dF}{d\phi} \nabla \phi - \nabla P + \rho g \mathbf{z} \right) \right] + q = 0. \tag{7}$$

Equation 7 represents a nonlinear diffusion equation describing the evolution of porosity caused by fluid injection and production in the reservoir. Equation 7 generalizes the poroelastic model, for if $F(\phi)$ in equation 6 is a linear function

$$F(\phi) = C_\ell \phi + D_\ell, \tag{8}$$

where C_ℓ and D_ℓ are constants, we recover a linear diffusion equation

$$\frac{\partial \phi}{\partial t} + \nabla \cdot \left[\frac{k}{\mu} (C_\ell \nabla \phi - \nabla P + \rho g \mathbf{z}) \right] + q = 0. \tag{9}$$

The irreversibility, which is a key feature of poroplastic behavior, is tied to the maximum effective pressure (p^*) to which the reservoir rocks have been subjected (Chen and Mizuno, 1990; Audet and Fowler, 1992). In particular, if the effective pressure is increased by production to values which are larger than any previous effective pressure, the reservoir rocks deform along one pressure-porosity curve. However, if the effective pressure is reduced, a different pressure-porosity curve is followed, hence the irreversibility. The simplest mathematical representation involves two families of lines with distinct slopes (Barenblatt et al., 1990). The particular family governing the behavior depends on the relationship of the effective pressure to the maximum effective pressure to which the rock has been subjected, p^*. Thus, $F(\phi)$ and its derivative depend on the size of p_e relative to p^*:

$$\frac{dF}{d\phi} = \begin{cases} K_1 & p_e < p^* \\ K_2 & p_e = p^* \end{cases}, \tag{10}$$

where K_1 is the slope of the curve when the effective pressure is less than the maximum effective pressure p^*, and K_2 is the slope of the curve for rocks on the normal consolidation line (Barenblatt et al. 1990). Note that in this model, if the effective pressure is always less than p^*, the reservoir material will deform linearly. Such a situation is invoked in our analysis of surface deformation at the Wilmington oil field.

Quasi-static deformation of the overburden induced by reservoir volume change

The equations discussed in the previous subsection describe processes occurring within the reservoir itself. In particular, equations 7 or 9 govern the evolution of porosity within a deformable reservoir caused by production. Actual observations pertain to the deformation of the overburden some distance above the reservoir proper. To interpret deformation data in terms of reservoir porosity and volume change, one must consider how the production-induced deformation propagates upward. We use a linear elastic model to describe the propagation of stress and strain through the overburden. That is, even though the reservoir may deform nonelastically, within a very short distance above the reservoir, the behavior is essentially elastic. Thus, we use an effective elastic source model, as is used in earthquake and explosion seismology (Aki and Richards, 1980), to represent the source. Effective elastic source models have also been used to image volume changes caused by volcanic processes (Vasco et al., 1988).

The governing equation for deformation ($\mathbf{u}$) within the overburden is (Vasco et al., 2000)

$$\frac{\partial}{\partial x_j} \left[G_e \left(\frac{\partial u_i}{\partial x_j} + \frac{\partial u_j}{\partial x_i} \right) + \lambda \frac{\partial u_k}{\partial x_k} \delta_{ij} \right] = \frac{\partial}{\partial x_j} [K_u v_f] \delta_{ij}, \tag{11}$$

where G_e is the shear modulus associated with the overburden, λ is the Lamé constant corresponding to the overburden, and δ_{ij} is the Kroneker delta function (1 when i equals j, and 0 otherwise). The Lamé constant may be written in terms of the shear modulus and Poisson's ratio (ν) as

$$\lambda = \frac{2\nu G_e}{1 - 2\nu}. \tag{12}$$

The quantity K_u is the bulk modulus of the overburden,

$$K_u = \frac{2G_e(1+\nu)}{3(1-2\nu)}, \tag{13}$$

and v_f is the fractional volume change within the reservoir. Note that the volume change v_f occurs on the right-hand side of equation 11 as a source term. As we shall see, this fact has important implications for the inverse problem, in which we infer fractional volume changes from observed surface displacements.

Estimation of reservoir flow properties using quasi-static deformation

In this section, we discuss the solution to the inverse problem. The goal is to find a reservoir model (permeability distribution) that is compatible with the observed surface displacements and injection and production rates. The estimation or inverse problem is broken into two steps, along the lines of the previous subsection. First, observed quasi-static displacements are used to infer the distribution of volume change within the reservoir. This inverse problem is governed by equation 11. Second, the volume (or corresponding porosity) changes are used to estimate permeability variations within the reservoir. Equation 7 (or equation 9 if the reservoir behaves as a poroelastic medium) is the relevant equation for this inverse problem.

Using overburden deformation to infer reservoir volume change

The details of inverting deformation for reservoir volume change have been discussed extensively in Vasco et al. (1988,

2000, 2002). The approach is based on equation 11, which constitutes the forward problem of computing surface displacement given prescribed volume changes. The volume change $v_f(\mathbf{x})$ within the reservoir only occurs on the right-hand side of equation 11 and does not multiply the displacement field. Thus, both the associated forward and inverse problems are linear in nature.

The inverse problem is frequently cast in terms of a Green's function solution to equation 11, as in Vasco et al. (2000). Typically, the Green's function is found either analytically or numerically by solving the system of equations for a specific medium. For example, an elastic half-space Green's function was given in Vasco et al. (1988), generalizing the work of Maruyama (1964) to allow for an arbitrary Poisson's ratio. A solution for a layered elastic half-space was given by Jovanovich et al. (1974). A perturbation method was developed by Du et al. (1994) to calculate solutions for a known medium subject to slight variations in elastic moduli. It is also possible to use a purely numerical solution, as discussed in Vasco et al. (2000). Assuming that an appropriate Green's function, $g_i(\mathbf{x}, \zeta)$, is available, we base our approach on the integral representation of the general solution of equation 11 (Aki and Richards, 1980):

$$u_i(\mathbf{x}) = \int_V v_f(\zeta) g_i(\mathbf{x}, \zeta) dV, \tag{14}$$

where ζ denotes the coordinates within the reservoir volume V.

Estimates of reservoir volume change are based upon a number of observations of surface deformation and a discrete version of equation 14. In the discrete version, we represent the reservoir volume by a set of N nonoverlapping rectangular cells or grid blocks. Each grid block in the reservoir model may undergo a distinct volume change. The details are given in Vasco et al. (1988, 2000, 2002), and we only present the resulting discrete set of equations, given M observation points $\mathbf{x}_j$:

$$u_i(\mathbf{x}_j) = \sum_{n=1}^{N} \Gamma^n{}_{ij} v_n = \mathbf{\Gamma}_{ij} \cdot \mathbf{v}, \tag{15}$$

where v_n is the average volume change for grid block n, and $\mathbf{\Gamma}_{ij}$ is a vector with N components:

$$\Gamma^n{}_{ij} = \int_{R_n} g_i(\mathbf{x}_j, \zeta) dV. \tag{16}$$

The index i runs from 1 to either 1, 2, or 3, depending on the type of data (leveling, tilt, GPS, InSAR), and j varies from 1 to M. Note that we may compute the coefficients $\Gamma^n{}_{ij}$ using either an analytical Green's function, such as for an elastic half-space, or numerically, using finite differences. In the finite-difference approach we need to solve the forward problem (equation 11) N times (once for each rectangular cell R_n). In each case, the right-hand side of equation 11 corresponds to point sources distributed over one of the rectangles R_n. Each forward run will provide the components for all observations.

The direct solution of a system of equations, comprised of linear constraints 15, is typically an unstable process, sensitive to numerical and modeling errors. In order to stabilize the inversion, we adopt a regularized least-squares procedure, as described in Vasco et al. (2000). Specifically, we minimize both the squared misfit to the observations and a penalty term. The penalty term is a measure of the deviation of the volume-change model from a prior model $\mathbf{v}_0$. In the application below, the prior model will be derived from reservoir injection and production data. The total penalized misfit function is given by

$$P(\mathbf{v}) = \|\mathbf{u} - \mathbf{\Gamma}\mathbf{v}\| + W_n \|\mathbf{v} - \mathbf{v}_0\|, \tag{17}$$

where $\|\cdot\|$ signifies the L_2 vector norm, and W_n is the norm penalty weight (Parker, 1994).

At this point, it might be worth commenting on the appropriateness of the prior model $\mathbf{v}_0$, which is based on net fluxes into the reservoir zones and on our formulation in general. Du and Olson (2001) stated that pressure changes represent a more direct and convenient variable for describing reservoir dynamics. However, a study by Castle et al. (1969) found that while subsidence could be linearly related to net liquid volume production, the correlation between reservoir pressure decline and subsidence was poor. Other investigators (Kumai et al., 1969; Shibasaki et al., 1969; Poland et al., 1975) have also found a linear relationship between subsidence and reservoir fluid fluxes. A linear relationship between fluid volume change and surface displacement is evident from equation 14. Castle et al. (1969) attribute the poor correlation with pressure to the fact that well pressures are unrepresentative of the average pressure decline within the formation as a whole. It is certainly true that well pressures are very sensitive to conditions directly around the borehole and well operations in general. Intuitively, it makes sense that, for a given fluid flux, the well pressure can vary dramatically depending on the condition of the borehole and the coupling of the well to the formation. Thus, averaged volumetric fluxes may be a more reliable quantity with which to constrain the inversion.

Permeability estimates based on reservoir volume change

The second step in the estimation of flow properties entails mapping the volume change into porosity variations ϕ and then into permeabilities. We assume that the fluid and grains are incompressible. Thus, the primary contribution to volume change within the rock is a change in porosity, which is driven by the introduction or expulsion of fluid. In this situation, the new porosity (ϕ) is related to the old porosity (ϕ_0) and the old (V_0) and new (V) volumes by the formula

$$V = V_0 + V_0(\phi - \phi_0). \tag{18}$$

Thus, the fractional volume change (v_f) is directly related to porosity changes ($\delta\phi = \phi - \phi_0$):

$$\delta\phi = \frac{\delta V}{V_0} = v_f. \tag{19}$$

In actual deformation caused by production and injection, the fractional volume change (and the corresponding change in porosity) will typically be a few percent each year.

We consider the porosity variations at two distinct times: t_0 and t_1. In the derivation, we consider linear equation 9, describing the evolution of porosity. As discussed below, such an equation seems appropriate for the application to Wilmington

field. Also, given sufficient time sampling, it is possible to consider time increments over which a linear approximation is appropriate. Consider the finite change in porosity over the time interval t_0 to t_1, denoted by $\delta\phi$. At each time (t_0 and t_1) the porosity satisfies equation 9, subject to the appropriate fluxes into the reservoir. For example, at time t_0, we have

$$\frac{\partial \phi_0}{\partial t} + \nabla \cdot \left[\frac{k}{\mu} (C_\ell \nabla \phi_0 - \nabla P + \rho g \mathbf{z}) \right] + q = 0. \quad (20)$$

Differencing the equations for times t_0 and t_1, and using the linearity of equation 9, we arrive at

$$\frac{\partial \phi_1}{\partial t} - \frac{\partial \phi_0}{\partial t} + \nabla \cdot \left[k \frac{C_\ell}{\mu} \nabla \delta\phi \right] + \delta q = 0, \quad (21)$$

where it is assumed that the pressure caused by the overburden and the fluid densities do not change and where δq denotes the change in reservoir fluxes.

Equation 21 depends on the intrinsic permeability k, the viscosity of the fluid μ, and the mechanical properties of the reservoir C_ℓ as well as the flow rates at times t_0 and t_1. If one has estimates of $\delta\phi$, μ, and C_ℓ and the time derivatives of ϕ_0 and ϕ_1, equation 21 may be thought of as an equation for the intrinsic permeability k. This idea was first discussed in Vasco et al. (2001) and applied to pressure and tilt data gathered during a shallow pumping test. Recently, the technique was modified and used to image reservoir permeability, based on time-lapse pressure estimates (Vasco, 2004). The approach is relatively straightforward and simply involves substituting estimates for $\delta\phi$, μ, and C_ℓ into equation 21. The result is a linear differential equation for k:

$$\nabla k \cdot \mathbf{\Phi} + k \nabla \cdot \mathbf{\Phi} = Q, \quad (22)$$

where

$$\mathbf{\Phi} = \frac{C_\ell}{\mu} \nabla \delta\phi, \quad (23)$$

and

$$Q = \frac{\partial \phi_0}{\partial t} - \frac{\partial \phi_1}{\partial t} - \delta q. \quad (24)$$

Equation 22 is then written in discrete form and solved using a regularized least-squares formulation, as was done in estimating reservoir-volume change. An alternative integral formulation was discussed in Vasco et al. (2001). Note that the coefficients of the equation for k depend on the porosity changes, $\delta\phi$, $\partial\phi_0/\partial t$, $\partial\phi_1/\partial t$, and the geomechanical response of the reservoir C_ℓ. Because these quantities are themselves estimates, there may be considerable modeling error in the coefficients. The sensitivity of estimates of k to errors in $\mathbf{\Phi}$ was explored by Vasco (2004). In the case of a transition between two steady states, one has $Q = -\delta q$ in equation 24.

APPLICATIONS

A synthetic test

We illustrate the method with an analysis of synthetic surface-displacement values, generated using a prescribed reference permeability model (Figure 1). The depth to the top of the reservoir is set at 1.5 km. The model contains generally higher permeabilities to the west and in the north-central region. The variation in permeability is more than three orders of magnitude. A reservoir simulator is used to compute the pressure changes caused by two years of production from 11 wells (Figure 2). The pressure changes are used in equation 4, with $Q = \infty$, $\alpha = 1$, $\nu = 0.25$, and $G = 0.05 \times 10^5$ MPa to compute porosity changes. The porosity changes are mapped into fractional volume changes using equation 19. The fractional volume changes are converted into surface displacements using equation 14 and an elastic half-space Green's function from Vasco et al. (1988). These calculated values constitute the synthetic displacements used in this test.

The synthetic displacement values are first inverted for reservoir volume change. The reservoir is represented as a single layer, divided into a 53 × 27 grid of cells. The penalized misfit function (equation 17) is minimized using the iterative least-squares solver LSQR (Paige and Saunders, 1982). As indicated in equation 19, the fractional volume change maps directly into porosity changes. The changes in porosity are then used in equations 22, 23, and 24 to estimate reservoir permeability variations. The porosity changes occur between two static states, so the temporal derivatives in equation 24 vanish. Again, a penalized least-squares formulation is used to estimate the permeabilities. A more detailed description of this approach may be found in Vasco (2004). The resulting

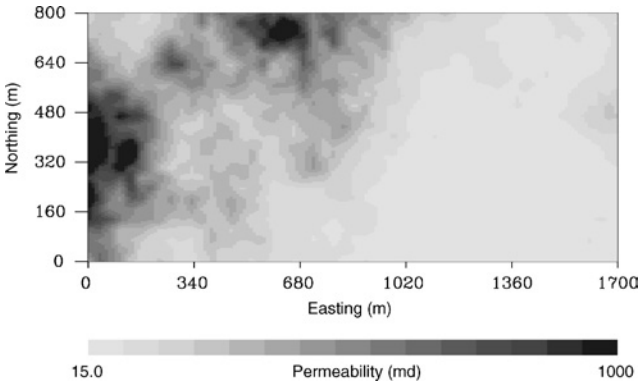

Figure 1. Spatial permeability variation used to generate a set of surface displacement values. The gray scale denotes the permeability variations within the reservoir model.

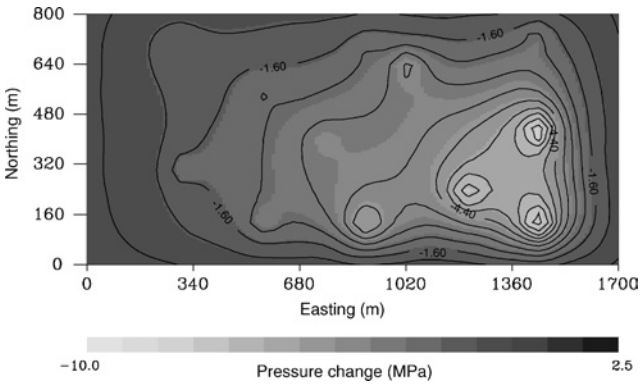

Figure 2. Pressure changes after two years of production from the reservoir model.

permeability model (Figure 3) contains the large-scale heterogeneity observed in the reference model (Figure 1).

Application to permanent scatterer observations from Wilmingtion field, California

In this subsection, we describe an application of the methodology to both leveling and InSAR observations from the Wilmington oil field in California. The InSAR data are processed to define permanent scatterers, objects whose scattering properties do not change significantly over a prescribed time interval (Ferretti et al., 2000, 2001). By restricting our attention to such permanent scatterers, we can obtain greater accuracy, on the order of a few millimeters. In addition, in areas containing a dense distribution of scatterers, we achieve high spatial resolution.

Geology and geomechanics of Wilmington field

The Wilmington field, located in the Los Angeles Basin, is one of a chain of oil fields overlying a basement high extending from Torrance field to the Huntington Beach offshore pool (Colazas and Strehle, 1994). The field is composed of heterogeneous turbidite sands which were subsequently folded and uplifted, forming a southeast-trending anticline 5.3 km wide and 19 km long. The top of the anticline is truncated by an unconformity caused by the uplift. The Wilmington anticline is intersected by a number of normal faults, dividing the reservoir into hundreds of fault blocks, down-dropped wedges, and compartments (Norton and Otott, 1996). The depositional complexity of the turbidites, coupled with the numerous faults, results in a highly heterogeneous reservoir.

The sediments comprising the oil reservoir are poorly consolidated and subject to significant internal deformation as the pore pressure changes. Because of notable subsidence linked to reservoir production, an extensive set of laboratory investigations were conducted to determine the compressibility of the sediments (Converse Engineering Company, 1957; Colazas, 1971). A set of porosity-pressure curves from such tests are shown in Colazas and Strehle (1994). The laboratory results illustrate the irreversibility of deformation, and the difference between the primary compaction curve and the expansion caused by a decrease in confining pressure. The porosity change caused by secondary pressure changes is just a few percent. Colazas (1979) found that the bulk volume compressibility as a function of pressure was similar for the major production zones (Tar, Ranger, and Terminal zones). Furthermore, the secondary porosity change was fairly constant for each lithology (sand/shale) in each zone.

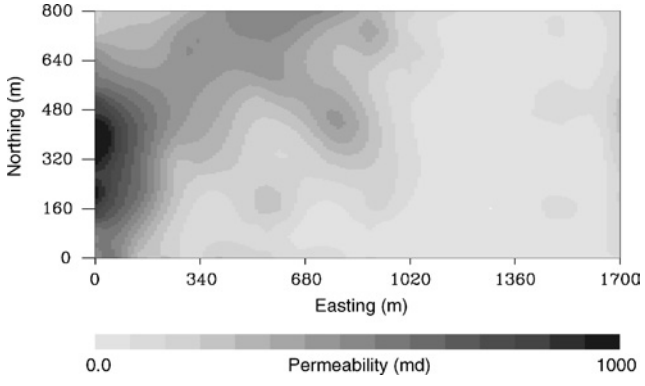

Figure 3. Permeability estimates resulting from an inversion of the surface displacement data.

Reservoir production

Wilmington field is the largest oil field in California and the third largest in the United States (Otott and Clarke, 1996). The field was discovered in 1932; by 1946, the major zones were under production. Current production is approximately 0.09 million barrels of oil and 1.1 million barrels of water per day from approximately 3670 wells (Colazas and Strehle, 1994). Current injection exceeds 1.3 million barrels per day into some 830 injection wells. An estimated 500 million barrels of reserves remain in the field. The majority of production is from four zones: the Tar, Ranger, upper Terminal, and lower Terminal (Colazas and Strehle, 1994), which consist of sands, siltstones, and shales. The total thickness of the oil-bearing formations in the Wilmington oil field is roughly 2 km.

Reservoir compaction and deformation

Surveys conducted during the 1940s revealed significant subsidence and horizontal displacements. By 1951, the subsidence, which assumed the shape of an elliptical bowl centered over the field, reached a maximum rate of more than 0.5 m/year (Colazas and Strehle, 1994). Cumulative subsidence between 1926 and 1967 totaled approximately 9 m, causing extensive damage to surface structures. By the 1960s, it was generally accepted that the cause of the deformation was oil and gas production from the underlying oil field. By 1961, full-scale water injection was begun in all four upper zones (Tar, Ranger, upper Terminal, and lower Terminal) in all fault blocks. Subsidence declined and ceased after only two years of water injection. Well profiles indicate that injected water entering the zones has excellent vertical distribution and that the total interval was expanding (Colazas and Strehle, 1994).

Currently, the City of Long Beach is responsible for arresting and preventing subsidence caused by oil and gas production. To this end, the city maintains an extensive network of approximately 900 benchmarks, which are surveyed semiannually (Colazas and Strehle, 1994). The surveys are accurate to roughly 1 cm of vertical displacement. These data indicate that measurable surface deformation is associated with the operation of the field. For example, a set of 452 elevation changes from 1994 to 1995 (Figure 4) contains peak variations of 5 to 10 cm.

At present, an empirical predictive tool, the roaming-tank model, is used to correlate net injection and elevation changes (Strehle, 1996). In essence, the technique constructs a moving-average estimate of net injection and production data within a specified radius (the tank) for each reservoir zone. The estimates are constructed on a quarterly basis, providing a measure of the time-varying fluxes into and out of the major zones in the field. The roaming-tank estimates of total injection from the first quarter of 1994 to the first quarter of 1996 are shown in Figure 5. A comparison of individual years indicates that

the net injection changes relatively slowly over this time interval. The correlation between net injection and subsidence is supported by the linear relationship between fluid flux and subsidence, noted by Castle et al. (1969).

Using leveling data to image reservoir volume change

A comparison of average volumetric fluxes into the reservoir provided by the roaming-tank model (Figure 5) and the observed surface deformation (Figure 4) reveals similarities as well as differences. The differences may be a result of the time intervals not being coincident. However, as noted above, the change in fluxes over this time interval is rather small. It is clear from the net production data (Figure 5) that the fluxes vary significantly from one reservoir zone to another. For example, the largest net volume fluxes are within the Tar and Terminal zones from 1994 to early 1996. Furthermore, there are notable differences in the pattern of injection and production in each zone.

In general, we would expect the surface deformation to be related to the fluid fluxes into and out of the reservoir. This raises the question, "Is it possible to find a model of reservoir volume change which is generally compatible with the reservoir fluxes and the surface deformation?" As is evident from equation 14, the observed surface deformation is a weighted spatial average of the reservoir volume change. The weighting is provided by the Green's function $g_i(\mathbf{x}, \zeta)$ and generally decreases as the distance between the volume change and the observation point increases. Note that, because of the heterogeneity and flow in the reservoir, the volume fluxes and reservoir volume changes do not have to coincide. For example, it is possible to have observable volume change where there is no net flux caused by injection or production if fluid propagates into some part of the reservoir.

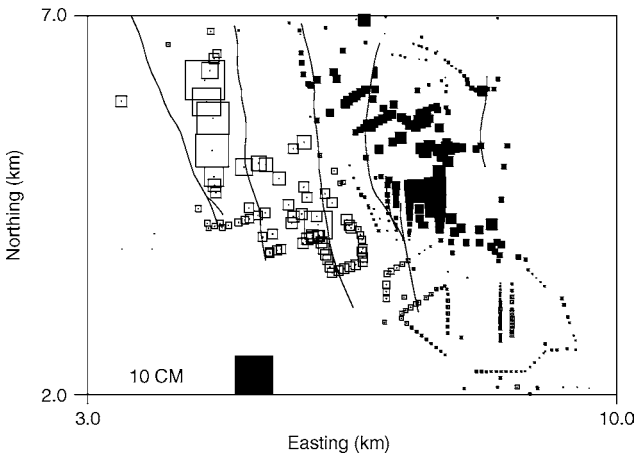

Figure 4. Vertical displacements over the one-year interval from 1994 to 1995. Each square is associated with a surveyed benchmark used in this study. Open squares indicate benchmark subsidence, filled squares indicate benchmark uplift. The lateral dimensions of each square are proportional to the vertical displacement of the corresponding benchmark. The filled square at the bottom of the figure indicates a reference value of 10 cm. The mean was removed from the displacement field before plotting.

In order to find a model of volume change compatible with both surface deformation and the roaming-tank volume estimates, we conduct a constrained inversion of the surface deformation for reservoir volume change, i.e., we minimize

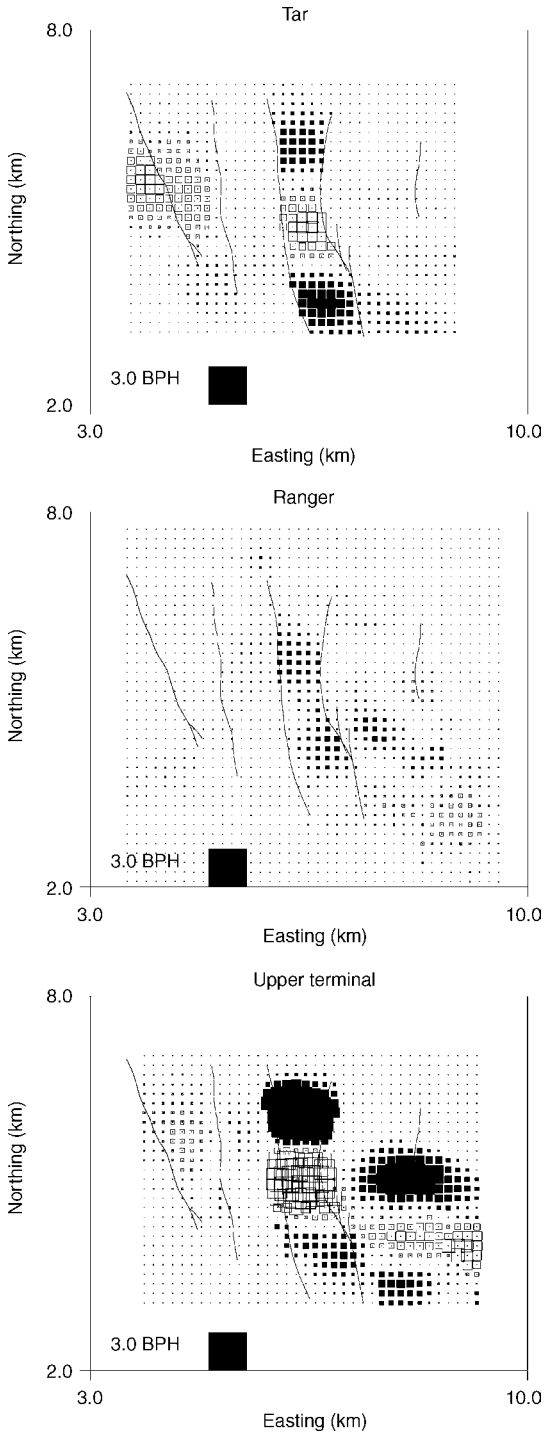

Figure 5. Net volume fluxes into the three main formations of the Wilmington reservoir, calculated using the roaming-tank model. Filled squares denote positive fluid fluxes, whereas open squares indicate withdrawal. The dimensions of each square are proportional to the net volume flux. The reference square represents a net fluid flux of 3.0 barrels per hour.

the penalized misfit function (equation 17). In this inversion, we constrain the volume change to be similar to the net volume fluxes, as calculated by the roaming-tank model (Strehle, 1996). Thus, the prior volume-change model $\mathbf{v}_0$ in equation 17 is derived from roaming-tank estimates. Specifically, the four quarters of data from the 1994–1995 time interval are integrated in each zone to compute $\mathbf{v}_0$. The inversion for reservoir volume change is along the lines of Vasco et al. (2000). That is, a three-layer reservoir model is constructed, in which the boundaries of the layers correspond to the interfaces between the Tar, Ranger, and upper Terminal zones. The interfaces in the reservoir model vary in depth, as described in Vasco et al. (2000). Each layer is divided into a 35 (east-west) $\times$ 25 (north-south) grid of cells, resulting in grid blocks of dimension 200 m $\times$ 200 m and variable thickness. The lateral boundaries of the grid coincide with those of Figures 4 and 5. The overburden is treated as an elastic half-space with a Poisson's ratio of 0.25, and the Green's function from Vasco et al. (1988) is used in equation 16.

A penalized least-squares formulation (equation 17) is adopted and the necessary equations for a minimum are solved using the LSQR algorithm of Paige and Saunders (1982). An unresolved issue is the value of the weight W_n that should be used in equation 17. The value of W_n controls how well we honor the prior model relative to fitting the leveling observations. We choose W_n by constructing a trade-off curve (Parker, 1994), which is a plot of data misfit against the misfit to the prior model, $\mathbf{v}_0$. This is done by conducting a sequence of inversions (15 in all) in which the value of W_n is systematically varied from a small value of 0.003 to a larger value of 0.173. For each inversion, we compute the total squared misfit to the leveling observations and the total squared misfit to the prior volume-change model. The trade-off curve, parameterized by W_n, is shown in Figure 6. We choose a compromise value, $W_n = 0.022$, which results in reasonable fit to the observations and, for the most part, honors the roaming-tank prior model $\mathbf{v}_0$. The resulting fits to the leveling data and the prior model are shown in Figure 7. Most of the leveling observations are fit to within the estimated error of 1 cm. Similarly, the estimated volume changes correlate well with the roaming-tank volume changes. There is some discrepancy for production and injection volume fluxes near zero (the inversion result has considerable scatter there). However, as noted above, as

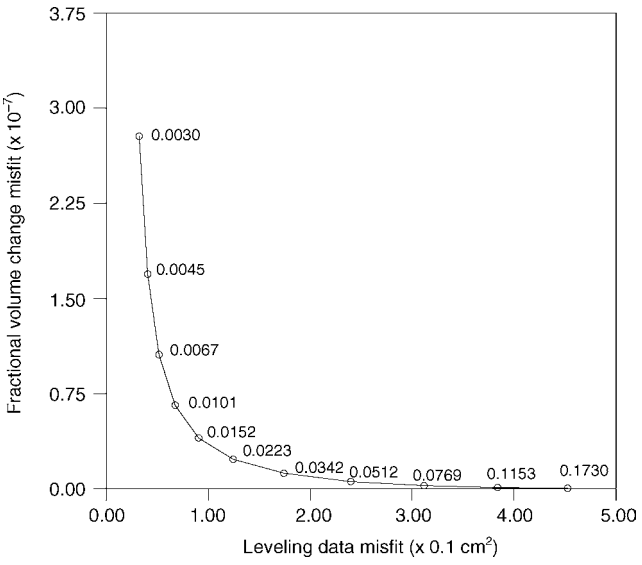

Figure 6. Trade-off curve derived from 11 distinct inversions. The curve represents squared misfit to the leveling data plotted against the squared deviation from the volume changes computed using the roaming-tank model. For each inversion, the norm weighting W_n in equation 17 was set to the value indicated at each point on the plot. The numerical factors in parentheses indicate the scaling of each axis (i.e., the values along each axis should be multiplied by the numbers in parentheses).

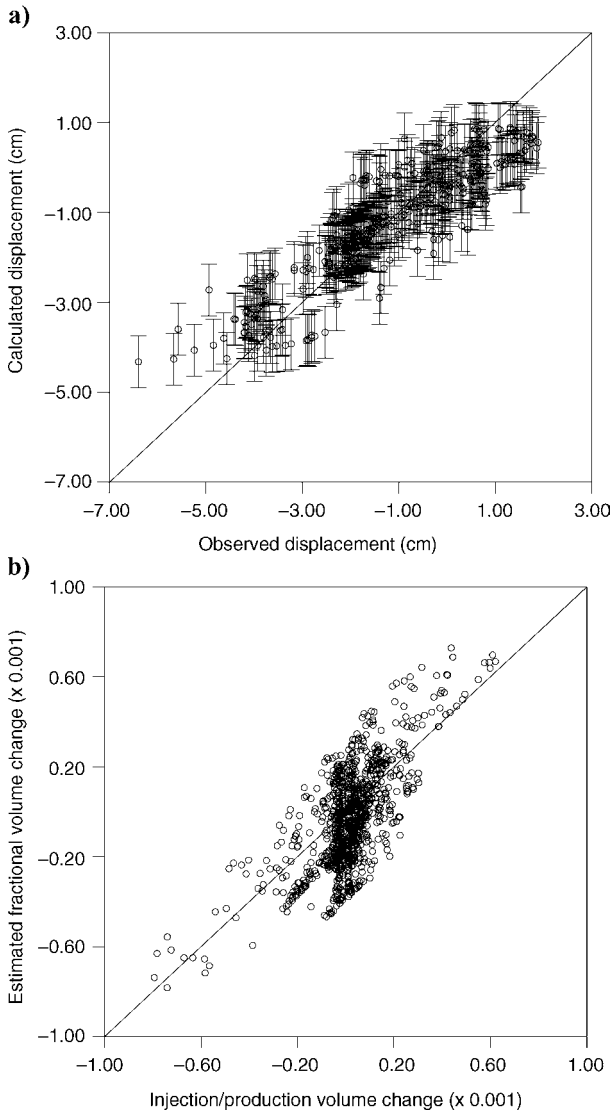

Figure 7. (a) Displacement values, calculated using the volume-change model, which resulted from the inversion. These values are plotted against the observed displacement values. For a perfect fit, the points would plot on the diagonal line shown. The errors bars signify one standard deviation. (b) Volume change obtained from the inversion plotted against the volume change from the roaming-tank model. The values along each axis should be multiplied by the numbers in parentheses.

a result of fluid migration and reservoir heterogeneity, we expect volume change at locations where there is little or no net injection or production. Thus, we would expect such scatter caused by fluid flow over the one-year interval.

The reservoir volume changes resulting from an inversion of the leveling data are shown in Figure 8. There are several interesting features to note in the inversion results. The volume changes vary in both magnitude and pattern for each zone, reflecting the influence of the prior roaming-tank model. This contrasts with the earlier results of Vasco et al. (2000) in which the pattern of volume change was similar for all depth intervals. However, the general depth-averaged pattern does correspond fairly well to the results of Vasco et al. (2000). There appears to be some degree of fault control on the volume change. For example, a significant volume increase in the Ranger zone appears to follow the curve of a crosscutting fault. Note that the inversion results are rather smoothly varying, even though no explicit roughness penalty was included. This is because of the relative smoothness of the prior roaming-tank model. We summarize this subsection by observing that it is possible to find a model of reservoir volume change that honors both the averaged production and injection data as well as the leveling observations.

Using InSAR observations to estimate reservoir volume changes

As shown in Vasco et al. (2000), the set of more than 500 leveling observations gathered semiannually by the City of Long Beach are a valuable asset in understanding the production-related changes in Wilmington field. However, new space-based techniques (in InSAR) can provide a highly accurate and significantly denser set of measurements (Bamler and Hartl, 1998; Massonnet and Feigl, 1998). The method is based upon interferometric phase shifts between radar reflections from two passes of an orbiting satellite. The phase shift can be unwrapped to produce precise estimates of range change, i.e., the change in distance from the reflection point to the observation point (the satellite). Range change is influenced by any displacement of the earth's surface, which has a nonzero projection onto the line-of-sight vector. For example, subsidence results in an increase in the distance to the satellite (Vasco et al., 2002). InSAR observations can potentially provide high spatial resolution, about 20 m $\times$ 20 m pixels for European Space Agency (ESA) ERS satellites. Furthermore, the theoretical accuracy of the technique is on the order of a few millimeters (Ferretti et al., 2001). The radar wave reflects at 23° from the normal to the earth's surface, making the range change very sensitive to vertical displacement.

The accuracy of InSAR range-change estimates is limited by temporal and geometric decorrelation and atmospheric inhomogeneity. Temporal decorrelation limits the application of InSAR to regions of the Earth for which the reflection characteristics do not change significantly over time. For example, changing vegetation will reduce the accuracy of InSAR estimates of range change. Geometric decorrelation and reflectivity variations as a function of the angle of incidence limit the number of image pairs that can be used. Finally, atmospheric variations induce traveltime perturbations for radar waves propagating from the satellite to the earth, introducing further error.

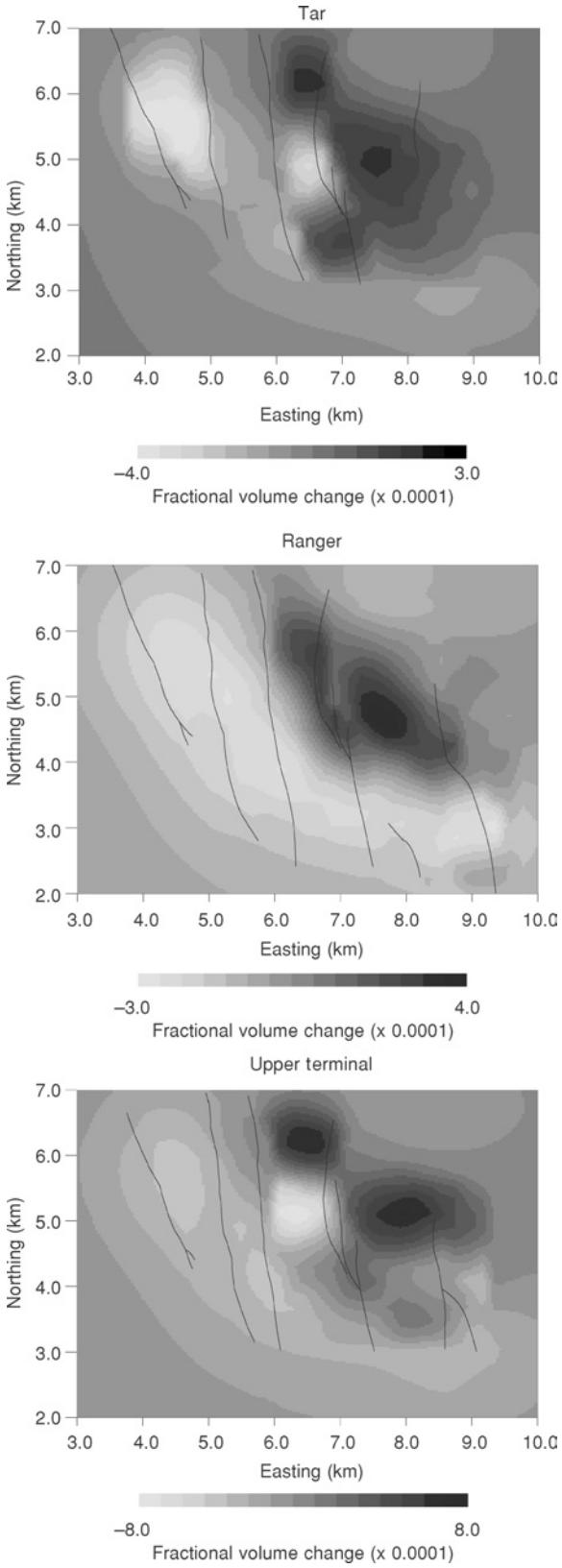

Figure 8. Volume change for the three layers of the Wilmington reservoir model. The solid black lines represent major interpreted faults in each layer. The scale values should be multiplied by the numbers in parentheses.

In the late 1990s, the SAR group of Politecnico di Milano proposed the permanent scatterer (PS) technique (Ferretti et al., 2000, 2001) to overcome problems caused by decorrelation and atmospheric effects. In essence, the approach is based on the identification of a class of objects, known as permanent scatterers, which have stable phase characteristics over long time intervals. In addition, when the dimensions of the scatterer are less than the resolution cell, geometric decorrelation is reduced and orbits with much larger separations may be used in the analysis. Lastly, atmospheric effects are removed by Wiener filtering, taking into account the different spectral behavior of motion and atmospheric phase components. The details of this procedure may be found in Ferretti et al. (2000, 2001) and Colesanti et al. (2003) and will not be repeated here.

Figure 9 displays the range change for a set of permanent scatterers defined over Wilmington field. These data are a subset of a more extensive collection of PS estimates from the Los Angeles basin, described in Colesanti et al. (2003). The color scale denotes motion along a line-of-sight vector extending from each pixel to the satellite. Positive values indicate motion in the direction of the satellite, converted to a rate. Thus, subsidence (i.e., motion away from the satellite) appears as negative values. The white regions indicate areas in which it was not possible to estimate motion by applying so-called standard PS analysis (Ferretti et al., 2001). For example, because of rapid motion in the Long Beach harbor area, permanent scatterers could not be defined there. Further processing can be used to estimate displacements in such regions. Alternatively, more conventional InSAR methods could possibly provide displacement values in rapidly moving areas, although with a higher corresponding error (Massonnet and Feigl, 1998). Permanent scatterers cannot be defined where water covers the surface, which is the case for much of the southern area in Figure 9. Note the high density of permanent scatterers over Wilmington field, approximately 17 0000 scatterers in all.

The surface deformation associated with the operation of the Wilmington oil field is apparent in Figure 9. In particular, the subsidence near the center of the figure and the uplift to the east. The pattern is in general agreement with the leveling data in Figure 4. The time interval (roughly eight years) is significantly longer for the estimates in Figure 9. The PS analysis derives an average velocity that will smooth over rapid fluctuations present in Figure 4. For example, the effects of a steamflood are visible at the left side of Figure 4. This region underwent significant uplift followed by equally significant subsidence (Vasco et al., 2000). On average, the uplift and subsidence almost canceled each other, resulting in much less net deformation.

Our analysis of the PS estimates is along the lines of our treatment of the leveling data. In particular, we are interested in the compatibility of the observed range changes (Figure 9) and injection/production in the major deforming zones of the reservoir. Unfortunately, we do not have roaming-tank estimates of volume flux for the entire interval 1992 to 2000. Thus, we must assume that the roaming-tank rates from 1994 to 1996 are representative of the longer injection and production schedule. In the future, we hope to have more extensive roaming-tank estimates, spanning the entire time interval. As with the leveling data, we first conduct a regularized least-squares inversion of the range-change observations. The Green's functions for the range-change observations are just weighted sums of the displacement Green's functions, as shown in Vasco et al. (2002). Thus, the formulation of the inverse problem for range-change data is virtually identical to that for displacements. As above, in order to estimate the weighting coefficient W_n used in equation 17, we construct a trade-off curve (Figure 10). The value of W_n producing

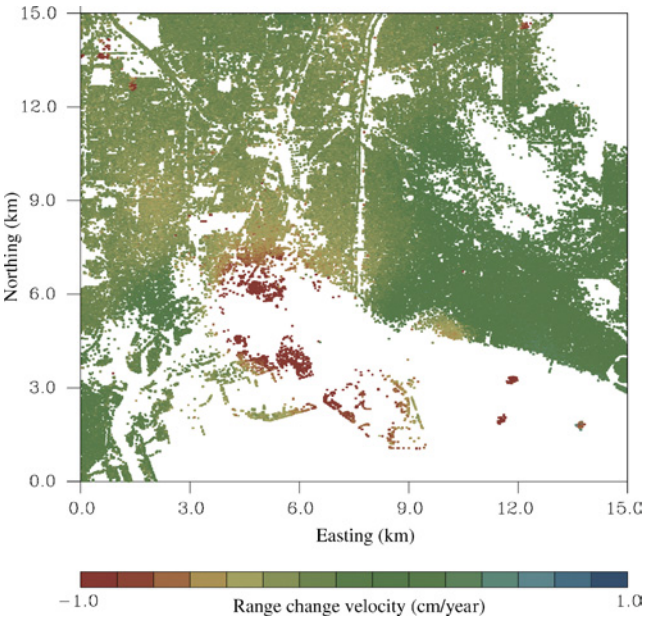

Figure 9. Permanent scatterer estimates of range change over the Long Beach region for the time period June 1992 to June 2000. The white regions indicate pixels for which displacements could not be determined.

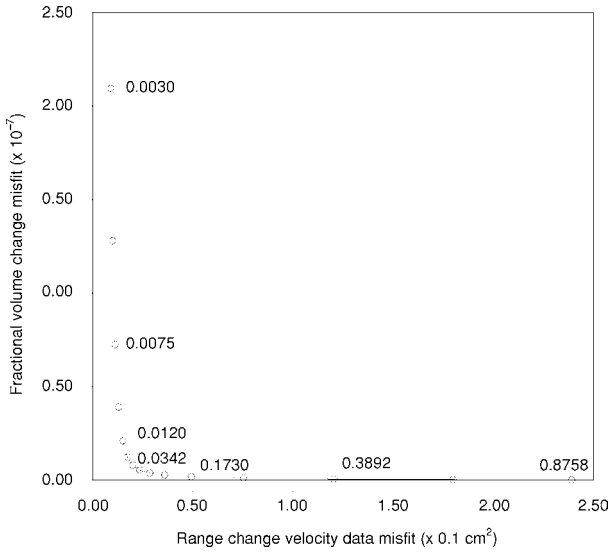

Figure 10. Trade-off curve derived from 15 distinct inversions. This figure is similar to Figure 6. For each inversion, the norm weighting W_n was set to the value indicated on the plot. The values along each axis should be multiplied by the numbers in parentheses.

relatively good fits to the data and honoring the injection and production rates lies at the sharp bend in the trade-off curve. The exact value used in the inversion was $W_n = 0.0342$. The resulting fits to the observations and the injection and production volume rates are shown in Figure 11. Overall, the fit to both measures is fairly good. There is scatter in the PS data fits, but, as is evident from Figure 9, the range-change estimates do contain notable isolated outliers. Such outliers cannot be fit by any model of volume change within the reservoir interval because of the averaging and smoothing nature of the Green's function and integral equation 14. For the most part, the range-change velocities are fit to within 5 mm/year. The correlation between injected and produced fluid volumes and the estimated reservoir volume change is also quite good. As in the case of the leveling data, there appear to be small amplitude variations in the estimated volume change associated with regions where the injection or production is close to zero. Again, this is consistent with fluid migration within the reservoir during the eight-year interval. That is, fluid is likely to migrate from injectors to other parts of the reservoir volume. Similarly, as pressure is reduced around a producer, the sediments some distance away from the production well can compact.

The resulting model of reservoir fractional volume change from 1992 to 2000 is shown in Figure 12. The distribution of v_f in Figure 12 is similar to that obtained from the 1994–1995 leveling data. However, there are differences between the leveling and PS models. For example, in the Tar zone, we do not observe a large volume increase in the eastern edge of the field, as was found in the inversion of the leveling data (Figure 8). In general, the PS inversion seems to contain smaller-scale features, perhaps due to the higher density of data. The

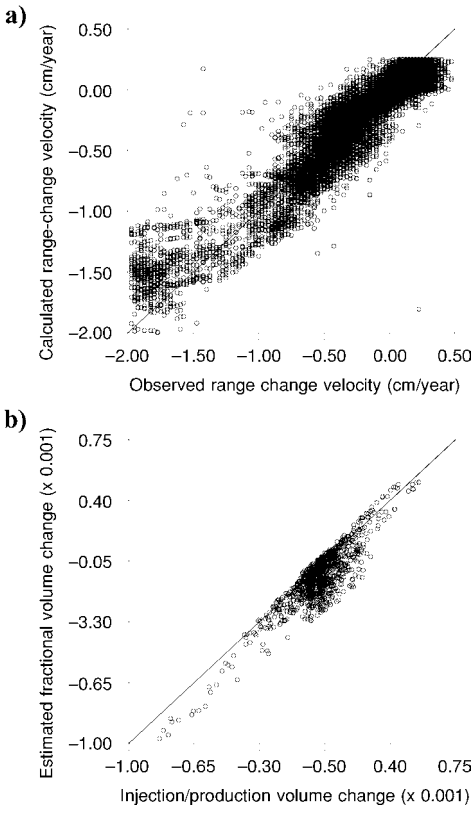

Figure 11. (a) Range-change values, calculated using the volume-change model, which resulted from the inversion. These values are plotted against the observed range changes. (b) Volume change obtained from the inversion, plotted against the volume change from the roaming tank model. The values along each axis should be multiplied by the numbers in parentheses.

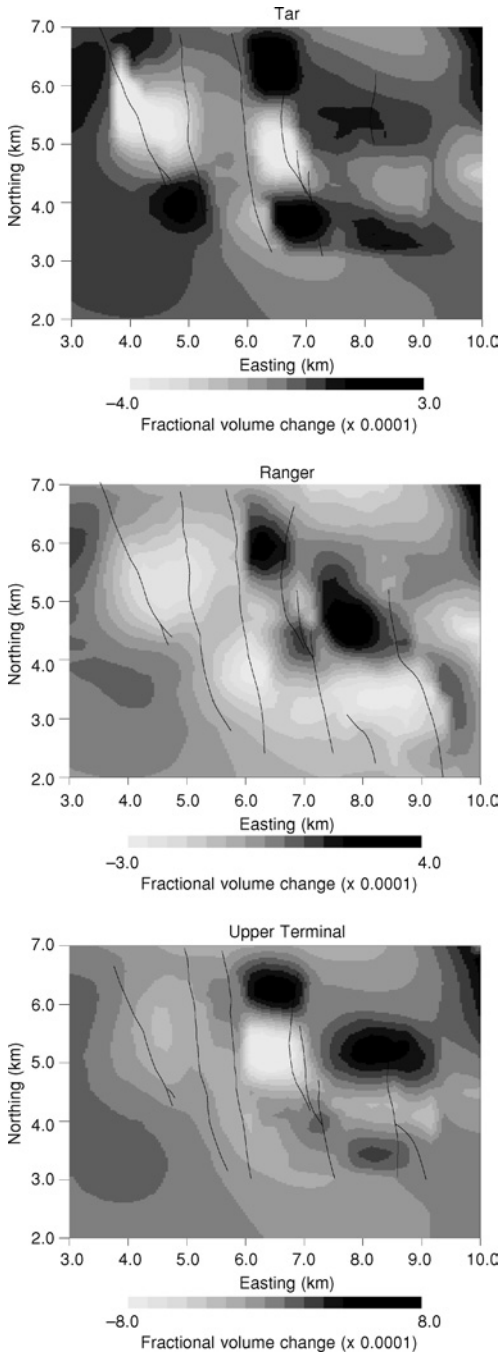

Figure 12. Results of the inversion of the permanent scatterer range-change estimates. Volume change for the three layers in the Wilmington reservoir model. The scale values should be multiplied by the numbers in parentheses.

overall agreement between the two inversions is encouraging, given the differences in the nature of the underlying data sets.

Inversion for reservoir permeability

Our estimation of reservoir permeability variations is based on equation 22 and the preceding model of reservoir volume change (Figure 12). At this point, we employ several assumptions to simplify the analysis. For example, we assume that the major zones (Tar, Ranger, and Terminal) are relatively isolated. That is, there is little flow between the major zones of the reservoir. This is a reasonable assumption, supported by years of production data. We also assume constant mechanical properties for each zone of the reservoir. Laboratory data (Colazas and Strehle, 1994) support the notion that the mechanical properties of the major zones are similar. In addition, tests indicate that sand and siltstone are approximately equally compressible (Colazas and Strehle, 1994). Pending more complete data on the variations in mechanical properties, we assume that the parameter C_ℓ in equation 23 is constant throughout the reservoir. In addition, because the volume change appears to vary slowly with time, we assume that the time derivatives in equation 24 vanish. Given sufficient temporal sampling of $\delta\phi$, we could solve for these derivatives, as was done by Vasco et al. (2001).

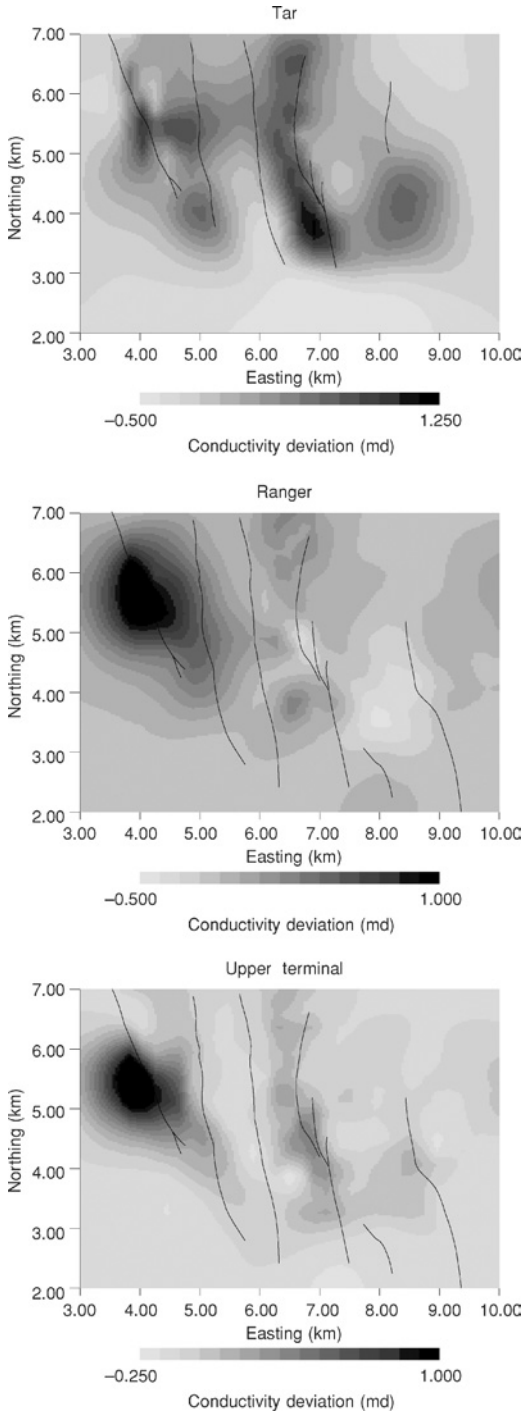

Figure 13. Permeability estimates for the three layers of Wilmington field. The deviations of permeability from an initial uniform model are shown in the figure.

The first step in the inversion is to discretize differential equation 22 using finite differences. The grid is identical to that used in the inversion for volume change, 35 (east-west) $\times$ 25 (north-south) cells for each layer (zone). The estimates of fractional volume change are combined with an estimate of C_ℓ from Colazas and Strehle (1994) and a composite viscosity for an oil-water mixture to compute Φ in equation 23. The change in flow rates are extrapolated from the roaming-tank quarterly averages to compute δq. Thus, we form the linear system for k, equation 22. As in Vasco (2004), we solve equation 22 using the iterative least-squares solver LSQR (Paige and Saunders, 1982). In order to stabilize the inversion, we included roughness and model norm penalty terms, as described in Vasco (2004).

The inversion algorithm is quite efficient, the entire procedure requiring only a few CPU seconds of computation. The resulting permeability deviations for the three major zones are shown in Figure 13. The permeability variations are with respect to an average background model. The deviations are normalized to unit variation. That is, unit variations are roughly equal to changes on the order of 100%. Values near -1 indicate a permeability near zero. For the most part, the deviations are greater than zero, indicating higher permeabilities overall. In the Tar zone, there is a corridor of high permeability roughly confined to a central fault block. Higher permeabilities are also found to the west of the field. In the deeper (Ranger and Terminal) zones, there are higher permeabilities to the west of the field and a band of somewhat higher permeability near the center of the field. There is some similarity between all three zones, suggesting that the calculated permeability may be controlled by the faults that cut across the entire reservoir. Finally, we note that the leveling data produce similar estimates of permeability heterogeneity (Figure 14). This suggests that the patterns are rather robust. It should be noted that the permeability estimates are linearly dependent on the reservoir fluxes, as is evident in equations 22 and 24. Thus, the estimates are influenced by the roaming-tank values shown in Figure 5. Any errors in these values will map into errors in the conductivity estimates. Better constraints (such as individual well information) should improve the conductivity estimates.

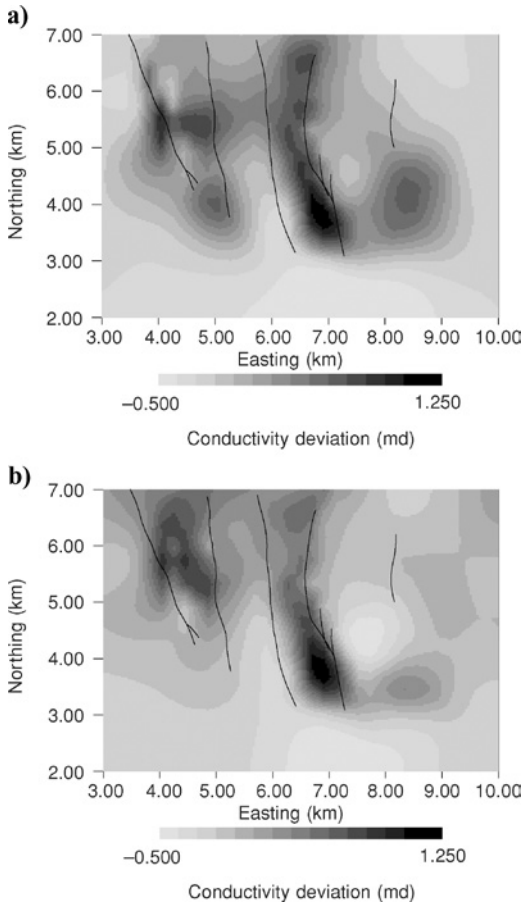

Figure 14. Comparison of permeability estimates made (a) using the permanent scatterer data and (b) based on the leveling data.

DISCUSSION AND CONCLUSIONS

To date, the published analyses of deformation within a reservoir in terms of production and injection have been rather limited. This is unfortunate because quasi-static deformation can improve our understanding of reservoir dynamics. Furthermore, new technologies such as the PS technique, inexpensive relative global positioning system (GPS) networks, and downhole tiltmeters are providing exciting new sources of data. In addition, time-lapse seismic surveys are imaging the displacement of layers overlying producing reservoirs. In this paper, we have developed an approach for mapping such deformation into flow-related volume and porosity changes. By introducing a penalty term, we find the volume changes that are most compatible with known injection and production schedules. Thus, we are able to assess the compatibility of the surface displacements with reservoir volumetric fluxes. Furthermore, using the estimates of porosity change and production information, we are able to infer large-scale variations in permeability within the reservoir. One advantage of the approach is that, if the reservoir behaves poroelastically, the inverse problem for permeability is linear. Furthermore, the algorithm for estimating permeability is extremely efficient. Field-wide estimates of permeability are calculated in only a few CPU seconds.

In the application to the Wilmington oil field, we assumed the overburden behaved as a linear elastic half-space. This was necessary because of our limited knowledge of the geomechanical properties of the individual layers overlying the reservoir. The half-space assumption is reasonable if the overlying layers do not contain any extremely stiff members, such as a thick carbonate sequence. All evidence suggests the overlying formations are relatively unconsolidated, as is the reservoir itself. The results presented here are encouraging: both leveling and satellite-derived InSAR observations are found to be compatible with the averaged reservoir injection and production volumes.

We made several approximations in order to estimate reservoir permeability. It was assumed that injected and produced fluids could be represented by a composite fluid with a single constant viscosity. This may be reasonable because of the long and extensive waterflooding at Wilmington field. Currently, some 1.3 million barrels per day are injected into the reservoir, and 1.1 million barrels per day of water are produced. This contrasts with the 0.09 million barrels of oil produced each day. Thus, the flow is probably dominated by the movement of water through the reservoir. We also assumed that the reservoir behaved as a linear poroelastic medium with constant mechanical properties. Certainly, in the early days of primary production, Wilmington field behaved like a poroplastic medium. The pore pressure was lowered substantially from existing values, resulting in large strains, over 9 m of subsidence. However, since full-scale water injection began in the early 1960s, the reservoir pressure has been maintained at a higher overall pressure. Thus, it is reasonable to assume that the effective pressure of the reservoir is greater than the maximum effective pressure p^* experienced in the early life of the field. Furthermore, the current surface deformation is of the order of several centimeters per year, which is compatible with small strains and porosity changes of only a few percent. Finally, laboratory data indicate that the mechanical properties of the reservoir rocks do not vary significantly, certainly much less than one order of magnitude. This is due to the unconsolidated nature of the reservoir rocks. The formations are also highly heterogeneous, composed of turbidites deposited in a deep basin. Thus, the overall behavior will be an average of this complicated lithology.

In general, it is difficult to resolve variations in reservoir volume change in depth. Thus, our estimates of permeability are really averages over large intervals within each reservoir zone. Furthermore, there will be trade-offs between volume change in the three zones of Wilmingtion field (Tar, Ranger, and Terminal). We used production and injection data to regularize the inverse problem for reservoir volume change. That is, we derived a model of reservoir volume change which is compatible with known production data. This form of regularization allowed us to match both the quasi-static deformation and the production data. It would be useful to apply this methodology to a field with more detailed records of injection and production.

This study represents an early attempt at reconciling reservoir production and surface deformation data. Several enhancements are possible and could be implemented in future studies. For example, more data could help constrain the estimates of volume change. To this end, it is possible to combine ascending and descending satellite observations,

obtaining two combinations of displacement components per station. The additional component improves the resolution of subsurface volume change. Multiple types of data, such as GPS, leveling, and InSAR may be combined into a single inversion. Downhole pressure data may be combined with surface deformation observations. Such a joint inversion can measurablely improve the resulting model. Furthermore, data from time-lapse seismic surveys could be used in conjunction or in place of surface deformation measurements. Time-lapse seismic data could potentially provide much more detailed depth resolution and may be used to separate velocity changes in the overburden from kinematic effects. The use of time-lapse seismic data extends the methodology to offshore oil fields, as does the use of time-lapse bathymetry data.

The modeling could be improved in several respects. For example, we could allow for a permeability which depends on pressure. The geomechanical properties of the reservoir could also be allowed to vary in space, given the appropriate data. An important aspect of any inversion are the uncertainties associated with the estimates. While the mapping from errors in the deformation data to errors in the volume change estimates is linear, the mapping into flow properties is not strictly linear. Specifically, estimating flow properties such as permeability, is based upon the solution of linear equation 22 in which the coefficients, contained in Φ, depend on the volume change estimates. Thus, while the estimate of permeability is the solution of a linear system, the estimate depends nonlinearly on the volume-change estimates. We can adopt a perturbation approach to relate small deviations in volume-change estimates to perturbations in flow properties. Such a perturbation approach will be the topic of a future investigation. For the current study at the Wilmington oil field, the differences between the inversion of range change and leveling data (as shown in Figure 14) provides some idea of the variability of the conductivity estimates.

ACKNOWLEDGMENTS

This work was supported by the Assistant Secretary, Office of Basic Energy Sciences of the U.S. Department of Energy under contract DE-AC03-76SF00098. The permanent scatterer (PS) data were processed by Tele-Rilevamento Europa (TRE), a spin-off company of Politecnico di Milano, worldwide exclusive licensee of the PS technique. The authors wish to thank the European Space Agency for all satellite data used in this study and the entire TRE staff. Additional computations were carried out at the Center for Computational Seismology, Lawrence Berkeley Laboratory.

REFERENCES

Aki, K., and P. G. Richards, 1980, Quantitative seismology: Freeman and Sons.

Allen, D. R., and M. N. Mayuga, 1969, The mechanics of compaction and rebound, Wilmington oil field, Long Beach, California, USA, *in* L. J. Tison, ed., Land subsidence: Affaissement dul sol: Association Internationale d'Hydrologie Scientifique publication 89, **2**, 410–422.

Audet, D. M., and A. C. Fowler, 1992, A mathematical model for compaction in sedimentary basins: Geophysical Journal International, **110**, 577–590.

Bamler, R., and P. Hartl, 1998, Synthetic aperture radar interferometry: Inverse Problems, **14**, R1–R54.

Barenblatt, G. I., V. M. Entov, and V. M. Ryzhik, 1990, Theory of fluid flows through natural rocks: Kluwer Academic Publishers.

Barends, F. B. J., F. J. J. Brouwer, and F. H. Schroder, 1995, Land subsidence: A. A. Balkema.

Biot, M. A., 1941, General theory of three-dimensional consolidation: Journal of Applied Physics, **12**, 155–164.

Bruno, M. S., and R. A. Bilak, 1994, Cost-effective monitoring of injected steam migration using surface deformation analysis: Society of Petroleum Engineers Western Regional Meeting, **27888**, 397–412.

Castillo, W., S. Hunter, P. Harben, C. Wright, R. Conant, and E. Davis, 1997, Deep hydraulic fracture imaging: Recent advances in tiltmeter technologies: International Journal of Rock Mechanics and Mineral Science, **34**, 3–4.

Castle, R. O., R. F. Yerkes, and F. S. Riley, 1969, A linear relationship between liquid production and oil-related subsidence, *in* L. J. Tison, ed., Land subsidence: Affaissement dul sol: Association Internationale d'Hydrologie Scientifique publication 88, **1**, 597–604.

Chang, E., D. S. Marx, M. A. Nelson, W. D. Gillespie, A. Putney, L. K. Warman, R. E. Chatham, and B. N. Barrett, 2000, Long range active synthetic aperture sonar, results: Oceans 2000 Conference, paper DTW-9901-00002.

Chen, W. F., and E. Mizuno, 1990, Nonlinear analysis in soil mechanics: Elsevier.

Chilingarian, G. V., E. C. Donaldson, and T. F. Yen, 1994, Subsidence due to fluid withdrawal: Elsevier Science.

Chin, L. Y., and N. B. Nagel, 2004, Modeling of subsidence and reservoir compaction under waterflood operations: International Journal of Geomechanics, **4**, 28–34.

Colazas, X. C, 1971, Subsidence, compaction of sediments and effects of water injection, Wilmington and Long Beach offshore fields: M.S. thesis, University of Southern California.

———, 1979, Long-term forecast of compaction, subsidence, and necessary subsidence control operations, Wilmington oil field: Report to the Department of Oil Properties, City of Long Beach.

Colazas, X. C., and R. W. Strehle, 1994. Subsidence in the Wilmington oil field, Long Beach, California, USA, *in* G. V. Chilingarian, E. C. Donaldson, and T. F. Yen, eds., Subsidence due to fluid withdrawal: Elsevier Science.

Colesanti, C., A. Ferretti, C. Prati, and F. Rocca, 2003, Monitoring landslides and tectonic motions with the permanent scatterers technique: Engineering Geology, **68**, 3–14.

Converse Engineering Company, 1957, Report of tests on oil well cores, Wilmington oil field: Report to the Board of Harbor Commissioners, City of Long Beach.

Dale, B. A., G. M. Narahara, and R. M. Stevens, 1996, A case history of reservoir subsidence and wellbore damage management in the South Belridge diatomite field: SPE 35658, 101–113

de Marsily, G., 1986, Quantitative hydrogeology: Academic Press.

Du, J., and J. E. Olson, 2001, A poroelastic reservoir model for predicting subsidence and mapping subsurface pressure fronts: Journal of Petroleum Science and Engineering, **30**, 181–197.

Du, Y., P. Segall, and H. Gao, 1994. Dislocations in inhomogeneous media via a moduli perturbation approach: General formulation and two-dimensional solutions: Journal of Geophysical Research, **99**, 13767–13779.

Dussealt, M. B., R. A. Bilak, and L. Rothenburg, 1993, Inversion of surface displacements to monitor in-situ processes: International Journal of Rock Mechanics and Mineral Science, **30**, 1219–1222.

Evans, K. F., G. R. Holzhausen, and M. D. Wood, 1982, The geometry of a large-scale nitrogen gas hydraulic fracture formed in Devonian shale: An example of fracture mapping using tiltmeters: Society of Petroleum Engineers Journal, **22**, 755–763.

Ferretti, A., C. Prati, and F. Rocca, 2000, Nonlinear subsidence rate estimation using permanent scatterers in differential SAR interferometry: IEEE Transactions on Geosciences and Remote Sensing, **38**, 2202–2212.

———, 2001, Permanent scatterers in SAR interferometry: IEEE Transactions on Geosciences and Remote Sensing, **39**, 8–20.

Guilbot, J., and B. Smith, 2002, 4-D constrained depth conversion for reservoir compaction estimation: Application to Ekofisk field: The Leading Edge, **21**, 302–308.

Jovanovich, D. B., M. I. Husseini, and M. A. Chinnery, 1974, Elastic dislocations in a layered half-space — I. Basic theory and numerical methods: Geophysical Journal of the Royal Astromical Society, **39**, 205–217.

Kumai, H., M. Sayama, T. Shibasaki, and K. Uno, 1969, Land subsidence in the Shiroishi Plain, Kyushu, Japan, *in* L. J. Tison, ed., Land subsidence: Affaissement dul sol: Association Internationale d'Hydrologie Scientifique publication 89, **2**, 645–657.

Landro, M., 2001, Discrimination between pressure and fluid saturation changes from time-lapse seismic data: Geophysics, **66**, 836–844.

Lumley, D. E., R. A. Behrens, and Z. Wang, 1997, Assessing the technical risk of a 4-D seismic project: The Leading Edge, **16**, 1287–1291.

Maruyama, T., 1964, Statical elastic dislocations in an infinite and semi-infinite medium: Bulletin of the Earthquake Prevention Research Institute of the University of Tokyo, **42**, 289–368.
Massonnet, D., and K. L. Feigl, 1998, Radar interferometry and its application to changes in the Earth's surface: Review of Geophysics, **36**, 441–500.
Minkoff, S. E., C. M. Stone, S. Bryant, and M. Peszynska, 2004, Coupled geomechanics and flow simulation for time-lapse seismic modeling: Geophysics, **69**, 200–211.
Norton, T. F., and G. E. Otott, 1996, The stratigraphy of the Wilmington oil field, *in* D. D. Clarke, G. E. Otott, and C. C. Phillips, eds., Old oil fields and new life: A visit to the giants of the Los Angeles Basin: AAPG Pacific Section Guidebook 74, 23–35.
Otott, G. E., and D. D. Clarke, 1996, History of the Wilmington field — 1986–1996, *in* D. D. Clarke, G. E. Otott, and C. C. Phillips, eds., Old oil fields and new life: A visit to the giants of the Los Angeles Basin: AAPG Pacific Section Guidebook 74, 51–55.
Paige, C. C., and M. A. Saunders, 1982, LSQR: An algorithm for sparse linear equations and sparse linear systems: ACM Transactions on Mathematical Software, **8**, 195–209.
Palmer, I. D., 1990, Uplifts and tilts at Earth's surface induced by pressure transients from hydraulic fractures: SPE Production Engineering, **5**, 324–332.
Parker, R. L., 1994, Geophysical inverse theory: Princeton University Press.
Poland, J. R., B. E. Lofgren, R. L. Ireland, and R. G. Pugh, 1975, Land subsidence in the San Joaquin Valley, California, as of 1972: U.S. Geological Survey Professional Paper **437-H**, 1–77.
Rouffignac, E. P., P. L. Bondor, J. M. Karanikas, and S. K. Hara, 1995, Subsidence and well failure in the South Belridge diatomite field: SPE 29626, 153–167.
Shibasaki, T., A. Kamata, and S. Shinto, 1969, Hydrologic balances in the land subsidence phenomena, *in* L. J. Tison, ed., Land Subsidence: Affaissement dul sol: Association Internationale d'Hydrologie Scientifique publication 88, **1**, 201–214.
Spiess, F. N., C. D. Chadwell, J. A. Hildebrand, L. E. Young, G. H. Purcell, and H. Dragert, 1998, Precise GPS/Acoustic positioning of seafloor reference points for tectonic studies: Earth and Planetary Science Letters, **108**, 101–112.
Strehle, R. S., 1996, Recent developments in subsidence, *in* D. D. Clarke, G. E. Otott, and C. C. Phillips, eds., Old oil fields and new life: A visit to the giants of the Los Angeles Basin: AAPG Pacific Section Guidebook 74, 83–86.
Sulak, R. M., 1991, Ekofisk: The first 20 years: Journal of Petroleum Technology, October, 1265–1271.
Vasco, D. W., 2004, Seismic imaging of reservoir flow properties: Time-lapse pressure changes: Geophysics, **69**, 511–521.
Vasco, D. W., L. R. Johnson, and N. Goldstein, 1988, Using surface deformation and strain observations to determine deformation at depth, with an application to Long Valley Caldera, California: Journal of Geophysical Research, **93**, 3232–3242.
Vasco, D. W., K. Karasaki, and L. Myer, 1998. Inversion of surface tilt caused by fluid migration: Journal of Geotechnical and Geoenvironmental Engineering, **124**, 29–37.
Vasco, D. W., K. Karasaki, and C. Doughty, 2000, Using surface deformation to image reservoir dynamics: Geophysics, **65** , 132–147.
Vasco, D. W., K. Karasaki, and K. Kishida, 2001. A coupled inversion of pressure and surface displacement: Water Resourses Research, **37**, 3071–3089.
Vasco, D. W., C. Wicks, and K. Karasaki, 2002. Geodetic imaging: High resolution reservoir monitoring using satellite interferometry: Geophysical Journal International, **149**, 555–571.
Wright, C. A., 1998, Tiltmeter fracture mapping: From the surface and now downhole: Petroleum Engineering International, January, 50–63.
Wright, C. A., E. J. Davis, W. A. Minner, J. F. Ward, L. Weijers, E. J. Schell, and S. P. Hunter, 1998, Surface tiltmeter fracture mapping reaches new depths — 10,000 feet and beyond?: SPE **39919**.